Available online at www.sciencedirect.com
SCIENCE DIRECT®
Thermochimica Acta 406 (2003) 129–142
thermochimica acta
www.elsevier.com/locate/tca

Experimental investigation and modelling of heat capacity, heat of fusion and melting interval of rocks

R. Leth-Miller[a,b,*], A.D. Jensen[b], P. Glarborg[b], L.M. Jensen[a], P.B. Hansen[a], S.B. Jørgensen[b]

[a] *ROCKWOOL® International A/S, Hovedgaden 584, DK-2640 Hedehusene, Denmark*
[b] *Department of Chemical Engineering, Technical University of Denmark, Copenhagen, Denmark*

Received 17 June 2002; received in revised form 4 April 2003; accepted 8 April 2003

Abstract

The heat capacity and heat of fusion were measured for a number of minerals using differential scanning calorimetry (DSC). The DSC measurements showed that the heat of fusion for the minerals is very low compared to the heat of fusion for pure crystalline phases reported elsewhere.

A model for the melting behaviour of mineral materials in terms of melting interval, heat capacities and heat of fusion has been developed. The only model input is the chemical composition of the mineral material. The model was developed to be implemented in a detailed model of a cupola furnace, thus the focus for the development was not only precision but also to obtain a model that was continuous and differentiable.

The model is based on several different submodels that each covers a part of the heating and melting of rocks. Each submodel is based on large amounts of empirical data. Comparison of the model and the DSC measurements showed reasonable agreement for the model to be used when a fast estimate is needed and experimental data is not available.

Keywords: Heat capacity; Heat of fusion; Minerals; Melting point; Modelling

1. Introduction

In the production of ROCKWOOL® products, rock materials are melted and heated to about 1500 °C. The energy requirements for heating and melting the rocks and superheating of the melt from the individual rock materials are considerable and together with the melting interval are of importance for determining the thermal efficiency of the cupola.

Models and experimental work for description of heat capacity, heat of fusion and melting temperature interval for rock materials have been developed earlier. Nathan and van Kirk [1] describe the melting curve (solid fraction as function of temperature) using an empirical model that predicts the composition of a mineral material in terms of crystalline phases. The model contains equations for estimating the liquidus temperature for nine phases as function of chemical composition, and uses these to construct a solid fraction function by solidifying a melt of a given chemical composition.

Methods for calculating the heat capacity of solid (crystalline and amorphic) and liquid rock materials

* Corresponding author. Tel.: +45-4656-0300; fax: +45-4655-5990.
E-mail address: rasmus.leth.miller@rockwool.com (R. Leth-Miller).

0040-6031/$ – see front matter
doi:10.1016/S0040-6031(03)00248-X

Nomenclature

$c_{p,l}$	heat capacity of liquid rock material ($J\,g^{-1}\,K^{-1}$)
$c_{p,s}$	heat capacity of solid rock material ($J\,g^{-1}\,K^{-1}$)
f_s	solid fraction of a rock materials
ΔH_{fus}	heat of fusion ($J\,g^{-1}$)
T	temperature (K)
T_g	glass transition temperature (K)
T_m	temperature at the middle of the melting interval or melting point temperature (K)
[X]	cation mole fraction of element X

Greek letter

α	parameter in f_s model

based on their composition in terms of crystalline phases are described by Steppins et al. [2], and methods for calculating the heat of fusion of minerals based on their composition in terms of crystalline phases is described by Konnerup-Madsen [3]. These methods are simple weighted sums over the properties of each of the phases present in a mineral material.

The composition of mineral materials in terms of crystalline phases can be predicted by the CIPW method described by Best [4]. The CIPW method is an algorithm that estimates the crystalline phase composition based on the chemical composition taking 31 phases into account, but does not predict melting interval as the method of Nathan and van Kirk [1].

Experimental data of pure mineral crystals have been collected and published, e.g. by Howie et al. [5] and Bach and Krause [6]. Crystalline rocks consist of a number of phases that mixes during melting, but the heat of mixing is not well described in literature.

The purpose of this work is to obtain knowledge of the enthalpy requirements for heating, melting and superheating of different raw materials used in ROCKWOOL® production to be better able to improve the production process. Furthermore, the purpose is to obtain a predictive model that can be used in a detailed model of a stone wool producing cupola furnace [7] when experimental data is not available.

A model based on several submodels, where each describes a part of the heating, melting and superheating, is presented. The model aims at describing the heat requirements as function of temperature for heating a rock taking heat capacity, heat of melting and melting temperature interval into account. The model input is the chemical composition while the composition in terms of crystalline phases is estimated using an empirical correlation. The apparent heat capacities of nine mineral materials have been measured using DSC. The apparent heat capacity has other heat consuming or producing phenomena embedded such as melting, calcination of $CaCO_3$ and mixing of melt from different crystals. The DSC method is briefly introduced and the results of the measurements are presented. Finally, the empirical model is compared to the experimental data.

In this paper, the term crystalline describes solid materials that have been formed in such a way that ordered crystals have formed. The crystals within a particular material may have varying chemical composition. The term amorphic describes the solid materials formed in such a way that crystals have not form, i.e. the material is homogeneous and has glass-like properties. The term magmatic describes the inorganic materials of volcanic origin. The term minerals is a broader and less well defined term including materials consisting of inorganic oxides (such as SiO_2, CaO, etc.) including the magmatic materials.

2. Model

The energy used for heating, melting and superheating the raw materials/melt is an important factor for the cupola operation. For use in a mathematical model of the cupola, it is an advantage that the enthalpy function, $\Delta H_r(T)$, is continuous and differentiable over the entire temperature interval. Thus, the function proposed here is given by

$$\Delta H_r = \int_{298\,K}^{T} c_{p,s} f_s \,dT + \Delta H_{fus}(1 - f_s) + \int_{298\,K}^{T} c_{p,l}(1 - f_s)\,dT \quad (1)$$

where f_s is the solid fraction of the mineral at a given temperature, and $c_{p,s}$ and $c_{p,l}$ the specific heat capacities of solid and liquid and heat of fusion of the

rock material as function of temperature. f_s is approximated with

$$f_s = \frac{1}{2}(1 - \tanh(\alpha(T - T_m))) \quad (2)$$

The parameters α and T_m are model parameters that has to be estimated The parameter α has no physical interpretation, while T_m can be interpreted as the middle of the melting temperature interval, i.e. the temperature where 50% of the material is molten.

The tanh function was chosen in order to obtain a continuous and differentiable function that is easy to use in detailed mathematical models of complex systems such as a cupola furnace (see [7]) where the melting is only one of the necessary submodels.

Determination of the values of $c_{p,s}$, $c_{p,l}$, ΔH_{fus}, α and T_m are described in the following sections.

2.1. Melting temperature

2.1.1. Crystalline raw materials

The melting temperature is estimated with a model of magmatic crystallisation by Nathan and van Kirk [1], who consider the nine solid phases listed in Table 1 in their model. The basic concept of the model is to calculate the liquidus temperature, T_{liq}, of all the nine phases corresponding to the composition of a melt. A small amount of the phase with the highest T_{liq} is then removed from the melt and a new composition of the melt is calculated. Then a new set of T_{liq} is calculated, more is removed from the melt and so forth until all the melt has been removed. The melting temperature interval is then the interval where the solid fraction is $0 < f_s < 1$.

Table 1
The solid phases considered in the crystallisation model

Mineral	Abbreviation	Composition
Magnetite	Mag	(Fe, Ti)$_3$O$_4$
Olivine	Olv	(Mg, Fe)$_2$SiO$_4$
Hypersthene	Hyp	(Mg, Fe)SiO$_3$
Augite	Aug	(Ca, Na)(Mg, Fe)Si$_2$O$_6$
Plagioclase	Pla	(Ca, Na)(Si, Al)$_4$O$_8$
Orthoclase	Ksp	(K, Na)AlSi$_3$O$_8$
Quartz	Qtz	SiO$_2$
Leucite	Leu	KAlSi$_2$O$_6$
Nepheline	Nep	(Na, K)AlSiO$_4$

(X, Y) denotes solid mixture of X and Y.

Table 2
The expressions for the geometric mean of the essential cations in the solid phases

Mineral	Geometric mean
Magnetite	$\sqrt[3]{[Fe(II)][Fe(III)]^2}$
Olivine	$\sqrt[3]{([Mg]+[Fe(II)])^2[Si]}$
Hypersthene	$\sqrt{([Mg]+[Fe(II)])[Si]}$
Augite	$\sqrt[4]{[Ca]([Mg]+[Fe(II)])[Si]^2}$
Plagioclase	$\sqrt[5]{([Na]+[K])[Al][Si]^3}$
Orthoclase	$\sqrt[5]{[K][Al][Si]^3}$
Quartz	1
Leucite	$\sqrt[4]{[K][Al][Si]^2}$
Nepheline	$\sqrt[3]{[K][Al][Si]}$

The liquidus temperatures are calculated as

$$\begin{aligned} T_{liq,i} = {} & a_{0,i} + a_{1,i}[Al] + a_{2,i}[Ti] + a_{3,i}[Fe(III)] \\ & + a_{4,i}[Fe(II)] + a_{5,i}[Mg] + a_{6,i}[Ca] \\ & + a_{7,i}[Na] + a_{8,i}[K] + a_{9,i}\ \ln(GM_i) \\ & + a_{10,i}\sqrt{[Al]([Na]+[K])} \end{aligned} \quad (3)$$

where [X] represent the cation fraction of cation X in the melt, and GM_i is the geometric mean of the essential cations of phase i (see Table 2). The coefficients, $a_{j,i}$, are given by Nathan and van Kirk [1].

For each of the solid solutions (e.g. (Fe, Ti) in magnetite in Table 2), the composition is calculated from equilibrium constants for the cations, e.g. for magnetite the composition of the Fe(III)–Ti solid solution is calculated as

$$\frac{([Fe(III)]/[Ti])_{Mag}}{([Fe(III)]^2/([Fe(II)][Ti]))_{liq}} = k = 1.84 \quad (4)$$

The remaining solution expressions are given by Nathan and van Kirk [1]. It must be noted that plagioclase ((Ca, Na)(Si, Al)$_4$O$_8$) consists of a mix of albite (NaAlSi$_3$O$_8$) and anorthite (CaAl$_2$Si$_2$O$_8$). It is therefore only necessary to calculate the ratio between Ca and Na to determine the composition of plagioclase [8].

An example of a modelled solid fraction curve for the volcanic rock, gabbro (chemical composition given in Table 3) using the method of Nathan and van Kirk [1] is shown in Fig. 1. The figure shows that the first solid is formed at approximately 1220 °C when a

Table 3
Chemical composition of the minerals

	SiO_2	Al_2O_3	K_2O	Na_2O	CaO	NaCl	Fe_2O_3	FeO	MgO	Cr_2O_3	TiO_2	P_2O_5	MnO
Diabase	0.4950	0.1410	0.0110	0.0290	0.0690	0.0000	0.0000	0.1170	0.0960	0.0000	0.0210	0.0060	0.0000
Merox	0.1220	0.0200	0.0010	0.0010	0.4120	0.0000	0.0000	0.2310	0.1000	0.0000	0.0120	0.0050	0.0290
Basalt	0.4095	0.1135	0.0105	0.0385	0.1275	0.0000	0.0000	0.1150	0.1155	0.0000	0.0280	0.0080	0.0010
Gabbro	0.4935	0.1450	0.0010	0.0280	0.1365	0.0000	0.0000	0.0650	0.0870	0.0000	0.0075	0.0010	0.0010
Zuzel	0.3880	0.0800	0.0040	0.0060	0.0000	0.3440	0.0000	0.0030	0.0830	0.0000	0.0030	0.0000	0.0050
Bauxite	0.1010	0.5050	0.0040	0.0010	0.0170	0.0000	0.0000	0.1930	0.0020	0.0000	0.0000	0.0010	0.0010
Olivin	0.4130	0.0030	0.0000	0.0010	0.0010	0.0000	0.0000	0.0670	0.4970	0.0020	0.0010	0.0000	0.0000
Anorthosite	0.4860	0.2940	0.0030	0.0300	0.1370	0.0000	0.0150	0.0000	0.0070	0.0002	0.0020	0.0010	0.0002

liquid sample is cooled and all the material has solidified at approximately 1000 °C. The model of Nathan and van Kirk [1] considers only nine crystalline phases and thus fails to give a complete description of raw materials that contain crystals not represented among the nine. A consequence of this is that when most of the material has solidified in the model the remaining elements can (in some cases) not form any of the nine phases. The model of Nathan and van Kirk [1] can thus often not reach a solid fraction equal unity as seen in Fig. 1.

2.1.2. Amorphic phase

Amorphic materials do not melt as such, but the viscosity properties are chanced abruptly at a certain temperature range, the glass transition temperature, T_g [9]. The amorphic materials thus changes from solid to liquid form at the glass transition temperature. No reliable models for estimating the glass transition temperature has been published. A rough estimate is that [10]

$$T_g \approx \tfrac{2}{3} T_m \quad \text{(K)} \tag{5}$$

where T_m is the melting point of the crystalline material with the same composition. The melting point (or interval) can often not be calculated using the model of Nathan and van Kirk [1] described above, since the amorphic materials frequently have a low silicon content and therefore form other crystalline phases than those used in the above model Eq. (3). The glass

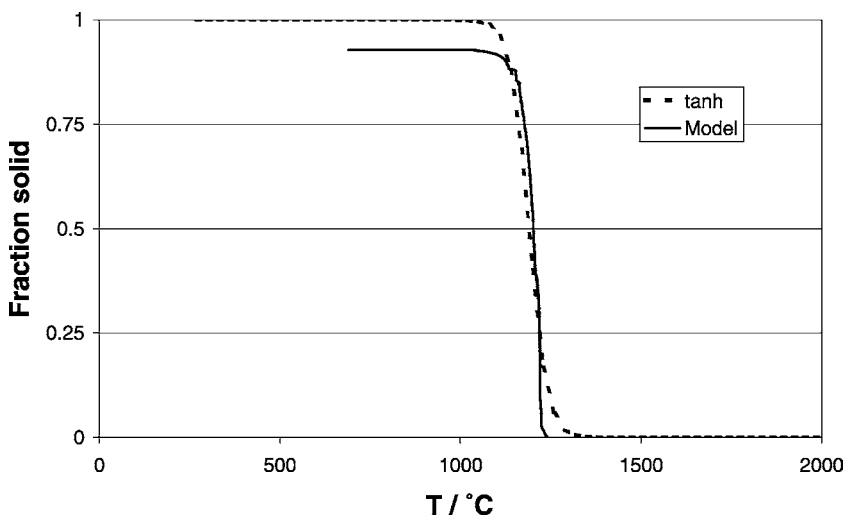

Fig. 1. Solid fraction of the volcanic rock, gabbro. Model by Nathan and van Kirk [1] and the fitted tanh in the f_s model plotted against temperature.

transition temperature must then be found in phase diagrams for each new material encountered.

2.1.3. Estimation of α and T_m

The two parameters in Eq. (2), α and T_m, can be estimated by comparing the function in Eq. (2) to the solid fraction function calculated with the model of Nathan and van Kirk [1] in the case of crystalline materials. Illustration of the solid fraction curve and fitting of the f_s function is shown in Fig. 1.

In the case of amorphic materials the T_m parameter in Eq. (2) is set equal to T_g and α must be adjusted to a value to obtain a reasonable value that depends on the what use the model is aiming at.

2.2. Specific heat capacity

2.2.1. Crystalline phase

Crystalline mineral materials consist of a number of mineral phases. The formal composition can be calculated from the total chemical composition with the CIPW method described by Best [4]. The CIPW method includes 31 different crystalline phases and is thus more detailed than the method of Nathan and van Kirk [1]. However, the CIPW method predicts only the formal composition of the solid mineral, and gives no information about the melting interval. The CIPW method is an algorithm that, based on the chemical composition, determines the formal amount of the each of the 31 crystals listed in Table 4 that are present in the mineral. The CIPW method is not ideal, because the temperature and pressure during the formation of the material, and thus the composition may differ substantially. The method is used despite this since it provides a fast method which is needed in especially the initial steps of process engineering work, i.e. for the first assessment raw material candidates in a production process or product design. The CIPW-norm has been used in a similar way by Conradt [11,12].

The heat capacity of the raw material can be assumed to be calculated as the weighted sum of the heat capacity of the phases [2]

$$c_{p,s} = \sum x_{\text{phase},i} c_{p,s,i} \quad (\text{J mol}^{-1}\,\text{K}^{-1}) \tag{6}$$

Correlations for the specific heat capacity for each phase are given in Tables 5 and 6. The correlations for c_p that are used in the model are only valid over a limited temperature range, but the correlations were used as a best guess beyond the range of validity. When the heat of fusion or heat capacity data for a crystal was not available (see Tables 5 and 6) the value for that crystal was set to the weighted average of the values for the other crystals present in the mineral.

Table 4
Names, abbreviations, chemical formulas and formula weights for the minerals [4]

Name (abbreviation)	Chemical formula	Formula weight
Quartz (Q)	SiO_2	60.1
Corundum (C)	Al_2O_3	102
Zircon (Z)	ZrO_2, SiO_2	183
Orthoclase (Or)	K_2O, Al_2O_3, $6SiO_2$	556
Albite (Ab)	Na_2O, Al_2O_3, $6SiO_2$	524
Anorthite (An)	CaO, Al_2O_3, $2SiO_2$	278
Leucite (Lc)	K_2O, Al_2O_3, $4SiO_2$	436
Nepheline (Ne)	Na_2O, Al_2O_3, $2SiO_2$	284
Kaliophilite (Kp)	K_2O, Al_20_3, $2SiO_2$	316
Halite (Hl)	NaCl	58.4
Thenardite (Th)	Na_2O, SO_3	142
Sodium carbonate (Nc)	Na_2O, CO_2	106
Acmite (Ac)	Na_2O, Fe_2O_3, $4SiO_2$	462
Sodium metasilicate (Ns)	Na_2O, SiO_2	122
Potassium metasilicate (Ks)	K_2O, SiO_2	154
Diopside (Di)	CaO, (Mg, Fe)O, $2SiO_2$	217–248[a]
Wollastonite (Wo)	CaO, SiO_2	116
Hypersthene (Hy)	(Mg, Fe)O, SiO_2	100–132[a]
Olivine (Ol)	2(Mg, Fe)O, SiO_2	141–204[a]
Dicalcium silicate (Cs)	$2CaO–SiO_2$	172
Magnetite (Mt)	FeO, Fe_2O_3	232
Chromite (Cm)	FeO, Cr_2O_3	224
Ilmenite (Il)	FeO, TiO_2	152
Hematite (Hm)	Fe_2O_3	160
Sphene (Tn)	CaO, TiO_2, SiO_2	196
Perovskite (Pf)	CaO, TiO_2	136
Rutile (Ru)	TiO_2	79.9
Apatite (Ap)	$3.3CaO–P_2O_5$	310
Fluorite (Fl)	CaF_2	78.1
Pyrite (Pr)	FeS_2	120
Calcite (Cc)	CaO, CO_2	100

[a] These two numbers represent the weights of the pure Mg- and Fe-end members, respectively.

Table 5
Heat of fusion, melting temperature and specific heat capacities for the minerals

Phase	ΔH_{fus} (kJ mol^{-1})	T_m (K)	a	b	c	d	e	Equation	Range (K)
Q	9.6 [6]		4.46030×10^{1}	3.77540×10^{-2}	0	1.00180×10^{6}		(a)	298–844 [5]
			5.89280×10^{1}	1.00310×10^{-2}	0	0		(a)	844–1800 [5]
C	107 [6]	2345 [5]	1.57360×10^{2}	7.18990×10^{-4}	9.88040×10^{2}	1.89690×10^{6}		(a)	298–1800 [5]
Z	144 [6]		2.36950×10^{2}	-1.78790×10^{-2}	-2.26780×10^{3}	-1.49600×10^{5}		(a)	298–1600 [5]
Or	158.9 [6]								
Ab	118.6 [6]								
An	146 [6]								
Lc	150.4 [6]		2.96840×10^{2}	2.68500×10^{-1}	0	4.32900×10^{6}		(a)	298–955 [5]
			3.92940×10^{2}	5.53320×10^{-2}	0	2.45220×10^{7}		(a)	955–1800 [5]
Ne	150.8 [6]		5.54800×10^{1}	5.90800×10^{-1}	0	0		(a)	298–467 [5]
			2.24180×10^{2}	1.34220×10^{-1}	0	0		(a)	467–1180 [5]
			3.44000×10^{2}	1.10400×10^{-2}	0	0		(a)	1180–1525 [5]
Kp	133.8 [6]		3.77760×10^{2}	1.10374×10^{-1}	-2.95740×10^{3}	0		(a)	298–810 [5]
Hl	28.158 [5]	1073.8 [5]	4.51510×10^{1}	1.79740×10^{-2}	0	0		(a)	298–1073.8 [5]
Th	23.723 [5]	1155 [5]	1.21930×10^{2}	8.14130×10^{-2}	0	0		(a)	514–1155 [5]
Nc	27.67874 [23]	1123 [23]	6.50000×10^{1}	2.10000×10^{-1}	0	0		(a)	298–723 [23]
			5.70000×10^{1}	1.50000×10^{-1}	0	0		(a)	723–1123 [23]
Ac									
Ns	51.82268 [23]	1362 [23]	1.53000×10^{2}	4.50000×10^{-2}	0	-3.50000×10^{6}		(a)	298–1362 [23]
	52.3 [6]								
Ks	50.2 [6]		1.41000×10^{2}	5.30000×10^{-2}	0	-2.00000×10^{6}		(a)	298–1200 [23]
Di	a	a	a	a	a	a	a	a	a
Wo	82.2		1.11250×10^{2}	1.43730×10^{-2}	1.69360×10^{1}	-2.77790×10^{6}		(a)	298–1400 [5]
	27.405 [5]	1817 [5]	1.07100×10^{2}	1.74810×10^{-2}	0	-2.29650×10^{6}		(a)	298–1700 [5]
Hy	a	a	a	a	a	a	a	a	a
Ol	a	a	a	a	a	a	a	a	a
Cs	168.1 [6]	2403 [5]	2.48710×10^{2}	-8.31450×10^{-4}	-2.05210×10^{3}	-9.07700×10^{4}		(a)	298–970 [5]
			1.34557×10^{2}	4.61080×10^{-2}	0	0		(a)	970–1710 [5]
Mt	138.072 [5]	1870 [5]	-3.55800×10^{3}	3.34730×10^{2}	-9.30900	2.53880×10^{-3}	1.42730×10^{5}	(b)	298–848 [5]
	138.1 [6]		9.68230×10^{1}	5.27330×10^{-2}	0	5.64130×10^{7}		(a)	848–1800 [5]
Cm			3.01840×10^{2}	4.15710×10^{-2}	1.14700×10^{-5}	-2.80270×10^{3}	4.87690×10^{5}	(c)	298–1800 [5]
Il	90.667 [5]	1640 [5]	-2.98950	6.50490×10^{-2}	2.42660×10^{3}	5.10570		(a)	298–1640 [5]
Hm	74.9 [6]	1895 [5]	-838.61	8.65250×10^{1}	-2.34340	6.05190×10^{-4}	2.78210×10^{4}	(b)	298–950 [5]
			-1.09570×10^{3}	2.72670×10^{-1}	3.39600×10^{4}	-1.02390		(a)	950–1800 [5]
Tn	123.805 [5]	1670 [5]	1.76730×10^{2}	2.38520×10^{-2}	0	3.99050×10^{6}		(a)	298–1670 [5]
Pf	112.1	2188 [5]	1.24960×10^{1}	4.51560×10^{-2}	2.46200×10^{3}	6.30180		(a)	298–1530 [5]
Ru		2103 [5]	6.30790×10^{1}	1.13070×10^{-2}	5.61600	9.86260×10^{5}		(a)	298–1800 [5]
Ap	224.8 [6]								
Fl	29.706 [5]	1691 [5]	-2.46920×10^{1}	5.80950×10^{-2}	1.87060×10^{3}	2.87740×10^{6}		(a)	298–1424 [5]
Pr			-2.03190×10^{1}	5.02990×10^{-2}	1.78700×10^{3}	-3.20020×10^{6}		(a)	298–1000 [5]
Cc			9.97150×10^{1}	2.69200×10^{-2}		2.15760×10^{6}		(a)	298–1200 [5]

The data for the components in the crystals are listed in Table 6. The correlations referred to in the table, Eqs. (a)–(c), are given by

$$c_p = a + bT + cT^{-0.5} + dT^{-2} \quad \text{(a)}$$

$$c_p = a + bT^{0.5} + cT + dT^{2} + eT^{-1} \quad \text{(b)}$$

$$c_p = a + bT + cT^{2} + dT^{-0.5} + eT^{-2} \quad \text{(c)}$$

[a] The crystals Di, Hy and Ol contains solid solution with varying compositions.

Table 6
Heat of fusion, melting temperature and specific heat capacitites for the minerals

Phase	ΔH_{fus} (kJ mol^{-1})	T_m (K)	a	b	c	d	e	Equation	Range (K)
Olivine									
Forsterite (Mg)	71.1 [6]	2163 [5]	2.27980×10^{2}	3.41390×10^{-3}	-1.74460×10^{3}	-8.93970×10^{5}		(a)	298–1800 [5]
Fayalite (Fe)	92.173 [5]	1490 [5]	1.72760×10^{2}	-3.40550×10^{-3}	2.24110×10^{-5}	0	-3.62990×10^{6}	(c)	298–1490 [5]
	92 [6]								
Diopside									
$CaMg(SiO_3)_2$	77.404 [5]	1664.5 [5]	1.91820×10^{2}	8.30790×10^{-2}	-2.17180×10^{-5}	0	4.27950×10^{6}	(c)	298–1600 [5]
	128.4 [6]								
$CaFe(SiO_3)_2$									
Hyperstene									
Clinoenstatite (Mg)	61.505 [5]	1830 [5]	2.05560×10^{2}	-1.27960×10^{-2}	-2.29770×10^{3}	1.19260×10^{6}		(a)	298–1600 [5]
	75.3 [6]								
Fe-enstatite	61.1 [6]								

The correlations referred to in the table, Eqs. (a) and (c), are given by

$$c_p = a + bT + cT^{-0.5} + dT^{-2} \quad \text{(a)}$$

$$c_p = a + bT + cT^{2} + dT^{-0.5} + eT^{-2} \quad \text{(c)}$$

Table 7
Coefficients for calculating the specific heat capacity of silicate glasses (400–1000 K)

	a_i	$b_i \times 10^2$	$c_i \times 10^{-5}$
SiO_2	66.354	0.7797	−28.003
TiO_2	33.851	6.4572	4.470
Al_2O_3	91.404	4.4940	−21.465
Fe_2O_3	58.714	11.3841	19.915
FeO	40.949	2.9349	−7.6986
MgO	32.244	2.7288	1.7549
CaO	46.677	0.3565	−1.9322
Na_2O	69.067	−3.2194	2.9101

$c_{p,\text{amorph}}$ and $c_{p,\text{cryst}}$ are the heat capacities at 700 K of amorphic and crystalline magma, respectively (data retrieved from [2]).

2.2.2. Amorphic phase

According to Steppins et al. [2], the heat capacity of amorphic minerals can be calculated as

$$c_{p,\text{amorph,s}} = \sum a_i x_i + \sum b_i x_i T + \sum c_i x_i T^{-2} \quad (\text{J mol}^{-1}\,\text{K}^{-1}) \tag{7}$$

where x_i are the mole fractions of the oxides. The coefficients are listed in Table 7.

2.2.3. Liquid phase

According to Steppins et al. [2], the heat capacity of liquid minerals can be calculated as

$$c_{p,\text{l}} = \sum x_i c_{p,i} \quad (\text{J mol}^{-1}\,\text{K}^{-1}) \tag{8}$$

where x_i are the mole fractions. The heat capacities are listed in Table 8.

Table 8
Specific heat capacity of liquid mineral materials (1200–1850 K)

	$c_{p,\text{l}}$ (J mol^{-1} K^{-1})
SiO_2	80.0 ± 0.9
TiO_2	111.8 ± 5.1
Al_2O_3	157.6 ± 3.4
Fe_2O_3	229.0 ± 18.4
FeO	78.9 ± 4.9
MgO	99.7 ± 7.3
CaO	99.9 ± 7.2
Na_2O	102.3 ± 3.6

The heat capacities are independent of temperature [2].

2.3. Heat of fusion

The heat of fusion of the amorphic mineral materials is zero, since it is a supercooled liquid. The heat of fusion of the crystalline mineral materials is calculated as the weighted sum of the heat of fusion of the phases [3]

$$\Delta H_{\text{fus}} = \sum x_{\text{phase},i}\, \Delta H_{\text{fus},i} \quad (\text{J mol}^{-1}) \tag{9}$$

The composition can be calculated from the total chemical composition using the CIPW method described by Best [4] and briefly described above. The heat of fusion for each pure phase is listed in Tables 5 and 6.

3. Measurement procedures

The experimental data in this work was obtained using differential scanning calorimetry (DSC). DSC has previously been used for measuring heat capacity, heat of fusion, melting interval and other transition quantities [13,14]. The materials that have been analysed by DSC include heavy metal fluoride glass [15], glass raw materials [16], pure metals [17], ashes and deposits from high-temperature coal–straw co-firing [18], ashes from solid fuel combustion [19] and polymers [13].

Differential scanning calorimetry is based on measuring the temperature difference between a sample and of a known reference material in a specified atmosphere while the samples are heated. The underlying assumption is that the heat transfer rate is proportional to the temperature difference between the surroundings and the sample/reference material, i.e. Fourier's law applies, and that the heat transfer coefficients are independent of material. Höhne et al. [20] discuss the theoretical background of DSC and provide an extensive introduction to practical DSC. Also Höhne et al. [20] describes how the heat capacity and transition heats are derived from the results. The problems using DSC, such as influence of kinetic effects at the fairly high heating rate, lack of homogeneity, etc. is discussed by Heide [21]. Evaporation of species [21] and chemical reactions [22] is known to be negligible from the stone wool production process and is thus omitted in this work except the calcination reaction.

The reference line is established by measuring approximately 20 mg sapphire in one crucible and approximately 20 mg α-aluminain the other. These materials were heated from room temperature to 1475 °C at 10 K min^{-1}. The crucibles are made of platinum and equipped with a lid that is not hermetically sealed. Subsequently, the sample is measured the same way as the sapphire, i.e. approximately 20 mg sample in one crucible and approximately 20 mg α-aluminain the other. The measurements were repeated to ensure homogeneity and tested with different particle sizes so that it had minimum effect.

From the heat capacity an enthalpy function can be obtained by integration as

$$H(T) - H(298.15\,\mathrm{K}) = \int_{298.15\,\mathrm{K}}^{T} c_p \,\mathrm{d}T \qquad (10)$$

4. Results and discussion

From the direct result of the measurements the heat capacity as function of temperature can easily be derived, but with the heat of fusion embedded. Fig. 2 shows an example of the resulting c_p curve (for gabbro). The value of the heat capacity at 500 °C is 1.3 J g^{-1} K^{-1}. A peak is observed at around 800 K and again at 1200 and 1500 K. The DSC measurements do not identify which transition a peak represents, but for the minerals investigated here it is known from the stone wool production that the melting point is above 1100 °C. The peaks at 800 and 1200 K are caused by transitions other than melting, e.g. recrystallisation, calcination of $CaCO_3$ or evaporation of crystal bound water (the mass signal indicate whether it is recrystallisation or calcination/evaporation). The peak at 1500 K correspond to the melting. The width of the peak indicates the melting temperature interval. The heat of fusion can be determined as the area under the peak of the resulting c_p curve (see an example in Fig. 2). Fig. 3 shows the measured apparent heat capacity of all the mineral materials included in this work. The measured range of the heat capacities is supported by values measured by Heide [21] of raw materials for silicate glasses that have a heat capacity of 1.5–2.0 J g^{-1} K^{-1}.

The raw materials included in these measurements are mainly of volcanic origin. The diabase, gabbro and basalt are volcanic magma materials that as groups differ by the crystal sizes which reflect how deep in the ground the were formed from the liquid magma. Merox and zuzel are foundry slags. Bauxite, olivine and anorthosite are other well-known materials [8,4]. The chemical composition of the materials are shown in Table 3.

Since the melting temperature interval is indicated by the resulting c_p curve the two parameters in Eq. (2) can be estimated. Fig. 4 shows the predicted melting curve and the c_p curve for a basalt. The model (Eq. (2))

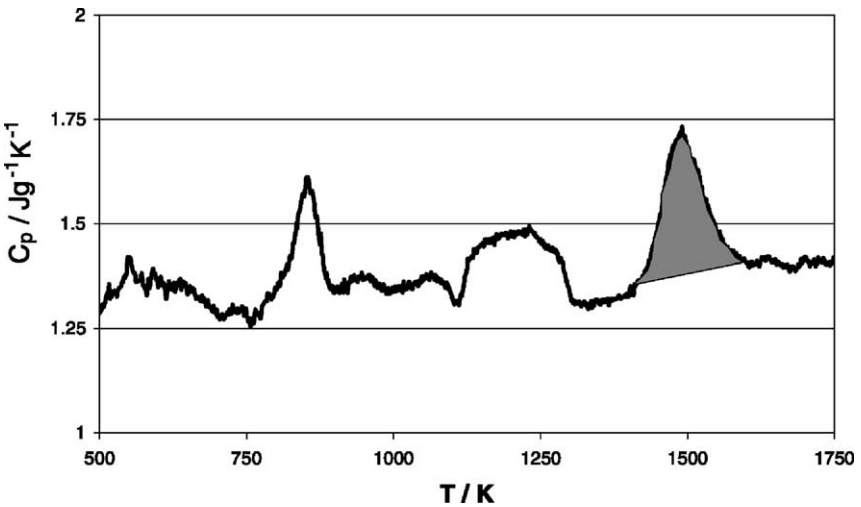

Fig. 2. The heat of melting (or other transition heats) can be extracted from the resulting head capacity function as the grey area, assuming that the heat capacity follows the base line of grey area.

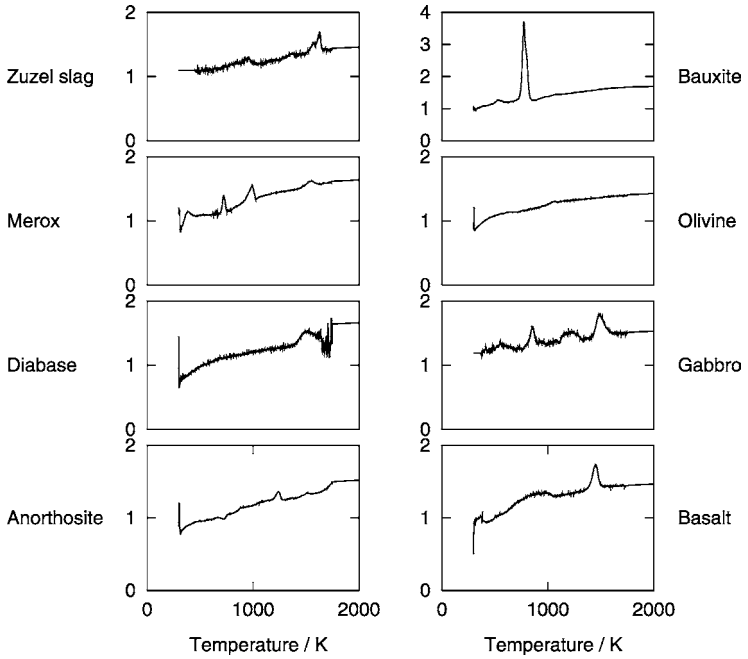

Fig. 3. Measured apparent heat capacity as function of temperature. The heat capacity is given in $J\,g^{-1}\,K^{-1}$.

is then manually tuned to the c_p curve and also plotted. The manual tuning is done so that the f_s function is (almost) unity below the melting interval and (almost) zero above. The melting interval is illustrated with the grey area in Fig. 2.

The measurements show some variance as illustrated with three measurements of gabbro (a mineral material) in Fig. 5. The curves are shifted vertically, however, the positions of the peaks are at the same temperature for all three measurements and the peaks

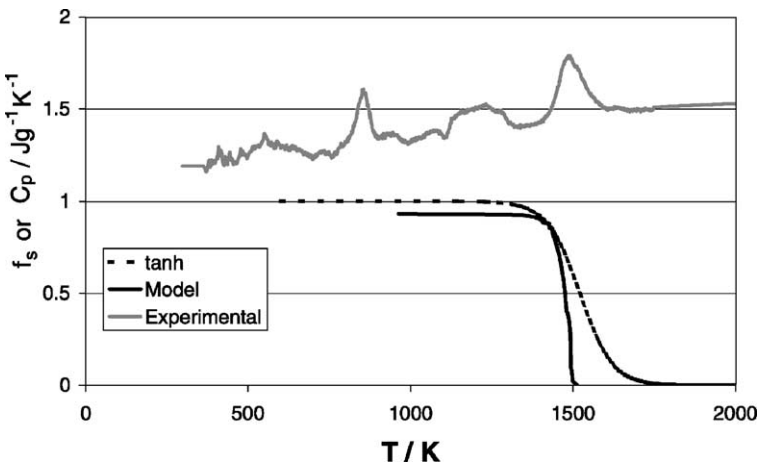

Fig. 4. Solid fraction of a gabbro (a mineral material) as function of temperature predicted by the melting model and the f_s model with fitted constants. Also the heat capacity from the DSC measurements is plotted on the solid fraction axis ($J\,g^{-1}\,K^{-1}$). The c_p curve was used to determine the parameters in the f_s model.

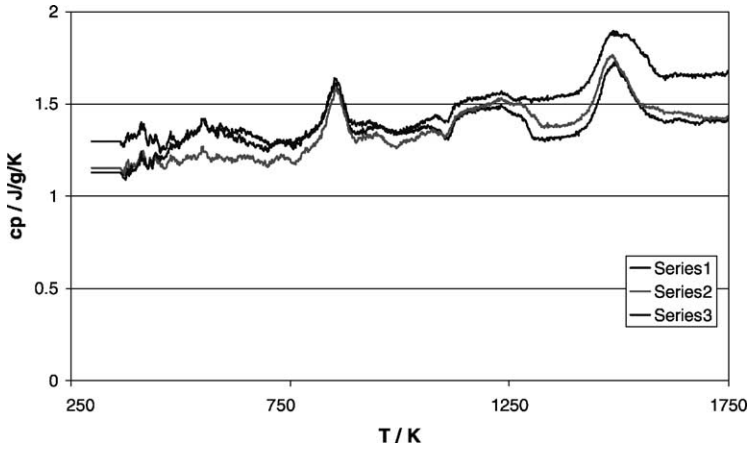

Fig. 5. Measured heat capacity of gabbro as function of temperature. The figure contains results of three independent measurements.

are of the same size (i.e. same height relative to the level of the specific heat capacity before and after the peak and the same width). The reason for the discrepancy is not clear.

The heat capacity plots in Fig. 3 shows that for all eight raw materials the heat capacity is slightly increasing with temperature, which is in good agreement with many other solids. Several of the plots show one or more peaks.

The plots for olivine and anorthosite have no peaks, indicating that no significant transitions take place, however, both materials did melt during the measurements, which must mean that the heat of fusion is almost zero. The plots for zuzel, diabase and basalt have each one peak at around 1500 K, which must be representing the melting of these three materials. Olivine, anorthosite, zuzel, diabase and basalt all have less than 1% mass loss during the measurements, and this small mass change is partly disturbances, since the mass also increases some time.

The heat capacity plot for bauxite in Fig. 3 shows one significant peak at around 850 K. At this temperature the mass is also observed to decrease approximately 14%. The peak thus most likely describe calcination which releases CO_2 from $CaCO_3$.

The heat capacity plot for merox show three peaks. The peaks at the melting point (1500 K) is very small. Two larger peaks are present at 750 and 1000 K. A mass loss of 7% was observed up to 750 K where after the weight was constant. The peak at 750 K may be release of crystalline water. The other peak may be a recrystallisation. Both peaks are, even though they are evident, not representing a large amount of energy.

The heat capacity plot for gabbro in Fig. 3 shows one significant peak at around 850 K. At this temperature the mass is also observed to decrease approximately 3%. The peak thus most likely describe calcination which releases CO_2 from $CaCO_3$.

When the solid fraction curve has been determined the modelled enthalpy function can be estimated using Eqs. (1), (6), (8) and (9). Fig. 6 shows the modelled enthalpy curve along with the measured (for gabbro). The plot shows good agreement between the modelled and the measured ΔH (evaluated through Eq. (10)) since the two curves are parallel both below and above the melting interval. However, the predicted heat of fusion is overestimated. On the experimental curve there is very little evidence of a heat of fusion. Fig. 6 shows the modelled enthalpy curve along with the measured, in the case where the heat of fusion has been set to zero in the model.

The very low heat of fusion was found for all the materials tested (Table 9). The best agreement between the model and the measurements was in all cases found when the heat of fusion was set to zero. Table 9 shows the energy requirements for each material for heating, melting and superheating from 25 to 1500 °C, both measured and predicted values (heat of fusion set to zero in the predicted values). Table 10 contains an overview of which phases the minerals contain according to the CIPW model. Anorthosite and zuzel slag are

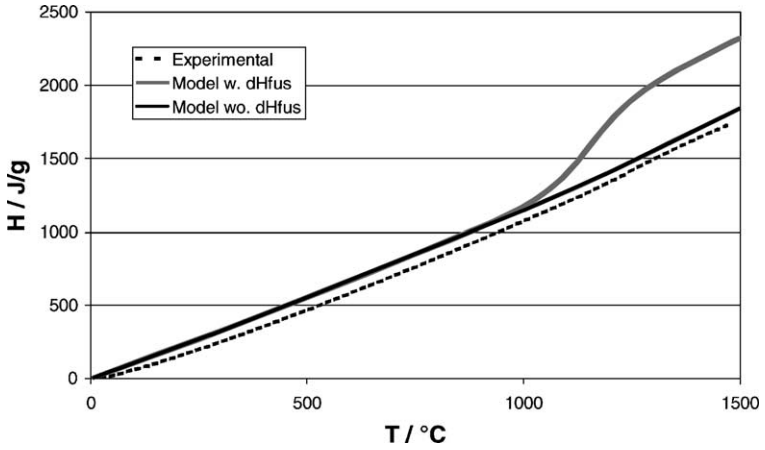

Fig. 6. The enthalpy, modelled and measured, plotted against temperature. The modelled curves are with and without the heat of fusion term, i.e. either the heat of fusion was estimated using Eq. (9) or it was set to zero.

the only two minerals containing quartz (Q) and they are the minerals for which the enthalpy model gives the largest positive error. Gabbro contains 49% anorthite (An) according to the CIPW model [4], but data was not found for the heat capacity of anorthite, and thus the accuracy of the prediction must be expected to be limited.

During the melting the chemical composition of the solid and liquid phase is assumed constant (equal to the total composition) in the model when the heat capacities are evaluated. This assumption will, however, only introduce a small error compared to the total energy needed for heating the minerals from 25 to 1500 °C.

The measurements showed that the minerals exhibited almost no heat of fusion. Other works (see Tables 5 and 6) demonstrate considerable heat of fusion of the crystalline phases that the minerals consist of. The different behaviour in the minerals may be caused by heat of mixing.

Table 9
Modelled and measured energy requirements, ΔH (heating from 25 to 1500 °C including melting), for a number of raw materials

	ΔH_{model} (J g^{-1})	ΔH_{exp} (J g^{-1})	Deviation (%)
Anorthosite	2463	1715	43.62
Basalt	1750	1896	−7.70
Bauxit	2212	2162	2.31
Gabbro	1685	2064	−18.36
Diabase	1812	1777	1.97
Merox	1825	1984	−8.01
Olivine	1869	1822	2.58
Zuzel slag	2110	1845	14.36

Table 10
Crystalline phases present in the minerals according to the CIPW model

	Q	C	Z	Or	Ab	An	Lc	Ne	Kp	Hl	Th	Nc	Ac	Ns	Ks	Di	Wo	Hy	Ol	Cs	Mt	Cm	Il	Hm	Tn	Pf	Ru	Ap	Fl	Pr	Cc
Anorthosite	x	x		x	x	x						x										x		x				x			
Basalt				x		x	x	x								x			x				x					x			
Bauxit		x				x	x	x	x						x													x			
Gabbro				x	x	x		x						x					x				x					x			
Diabase		x		x	x	x												x	x				x					x			
Merox						x	x	x	x										x	x			x					x			
Olivin		x			x	x						x							x			x	x								
Zuzel slag	x	x		x	x													x					x								

Available data

H	x	x	x	x	x	x	x	x	x	x	x	x		x	x	x	x	x	x	x	x	x	x	x	x	x		x	x		
cp	x	x	x				x	x	x	x	x	x		x	x	x	x	x	x	x	x	x	x	x	x	x	x		x	x	x

5. Conclusion

A model for predicting the melting behaviour of mineral materials in terms of melting interval and heat consumption based only on the chemical composition was developed. The model was compiled from a number of existing models that each describes part of the phenomenon.

A number of minerals relevant to production of ROCKWOOL® products have been investigated with DSC technique to obtain information about their melting interval, heat capacity and heat of fusion. The measurements showed that the minerals exhibited only very low heat of fusion.

The model has been compared with the experimental data and showed reasonable agreement when the heat of fusion was set to zero in the model. The model is not close to being an alternative to data, however, for fast estimates the model is usable. The model is not claimed to be a precise tool, but it can be useful for engineers.

The model was developed for use in a model of a mineral melting cupola furnace, where minerals are heated, melted and superheated from 25 to about 1500 °C. If the model is to be used for describing the phase transition precisely, the challenge of describing the heat of mixing should be addressed and the model should be refined with respect to both the f_s function and the evaluation of the heat capacities should be made dependent of the actual compositions of the solid and liquid phase during the melting.

Acknowledgements

This work is part of the research programme of ROCKWOOL® International A/S in co-operation with Computer Aided Process Engineering Centre (CAPEC) and Combustion and Harmful Emission Control (CHEC) at the Department of Chemical Engineering at the Technical University of Denmark. The project is funded by ROCKWOOL® and The Danish Ministry of Business and Industry.

References

[1] H.D. Nathan, C.K. van Kirk, A model of magmatic crystallisation, J. Petrol. 19 (1978) 66–94.

[2] J.F. Steppins, I.S.E. Carmichael, L.K. Moret, Heat capacities and entropies of silicate liquids and glasses, Contrib. Mineral. Petrol. 86 (1984) 131–148.

[3] J. Konnerup-Madsen, Energi-behovet ved opsmeltning af mineraler og bjergarter (Energy Requirements for Melting of Minerals and Rocks), Institut for Petrologi, Københavns Universitet, 1982 (in Danish).

[4] M.G. Best, Igneous and Metamorphic Petrology, Freeman, New York, 1982.

[5] R.A. Howie, B.S. Hemmingway, J.R. Fisher, Thermodynamic Properties of Minerals and Related Substances at 298.15 K and 1 bar (10^5 Pascals) Pressure and at Higher Temperatures, United States Government Printing Office, Washington, 1978.

[6] H. Bach, D. Krause, Analysis of the Composition and Structure of Glass and Glass Ceramics, Springer-Verlag, Berlin, 1999.

[7] R. Leth-Miller, A.D. Jensen, P. Glarborg, S.B. Jørgensen, L.M. Jensen, P.B. Hansen, Experimental investigation and mathematical modelling of a mineral melting cupola furnace, Ind. Eng. Chem. Res., in press.

[8] W.A. Deer, R.A. Howie, J. Zussmann, An Introduction to the Rockforming Minerals, 14th ed., Longman, Essex, UK, 1983.

[9] L.H. van Vlack, Elements of Material Science and Engineering, 6th ed., Addison-Wesley, Reading, MA, 1989.

[10] H. Scholze, Glas; Natur, Struktur und Eigenschaften, Springer-Verlag, Berlin, 1988.

[11] R. Conradt, A proposition for an improved theoretical treatment of the corrosion of multi-component glasses, J. Nucl. Mater. 298 (2001) 19–26.

[12] R. Conradt, A simplified procedure to estimate thermodynamic activities in multicomponent oxide melts, Molten Salt Forums 5–6 (1998) 155–162.

[13] E. Verdonck, K. Schaarp, L.C. Thomas, A discussion of the principles and applications of modulated temperature DSC, Int. J. Pharm. 192 (1999) 3–20.

[14] B. Wunderlich, A. Boller, I. Okazaki, K. Ishikiriyama, Heat-capacity determination by temperature-modulated DSC and its separation from transition effects, Thermochim. Acta 304–305 (1997) 125–136.

[15] R. Mossadegh, C.T. Moynihan, A.J. Bruce, M.G. Drexhage, DSC studies of melting behaviour of heavy metal fluoride glass compositions, Mater. Res. Bull. 22 (1987) 593–600.

[16] K. Heide, R. Franke, H.G. Schmidt, R. Straussberger, Investigation of the energy expended in heating glass raw materials to the melting temperature, J. Therm. Anal. 33 (1988) 615–618.

[17] N. Clavaguera, M.T. Clavaguera-Mora, J. Fontán, J.L. Touron, Melting vs. solidification of a pure metal analysed by DSC, Mater. Res. Soc. Symp. Proc. 481 (1998) 33–38.

[18] L.A. Hansen, F.J. Frandsen, K. Dam-Johansen, H.S. Sørensen, B.-J. Skrifvars, Characterisation of ashes and deposits from high-temperature coal–straw co-firing, Energy Fuels 13 (4) (1998) 803–816.

[19] L.A. Hansen, F.J. Frandsen, K. Dam-Johansen, H.S. Sørensen, Quantification of fusion in ashes from solid fuel combustion, Thermochim. Acta 326 (1999) 105–117.

[20] G.W.H. Höhne, W. Hemminger, H.-J. Flammersheim, Differential Scanning Calorimetry: An Introduction to Practitioners, Springer-Verlag, Berlin, 1996.
[21] K. Heide, Production planning in glass manufacture by means of thermal analysis, J. Therm. Anal. 38 (1992) 27–36.
[22] V.C. Kröger, Gemengereaktionen und Glasschmelze, Glasstechnishe Berichte 10 (1952) 307–324.
[23] L.B. Pankratz, J.M. Stuve, N.A. Gocken, Thermodynamic Data for Mineral Technology, Bulletin 677, United States Department for the Interior, Bureau of Mines, 1984.